Bone 125 (2019) 1–7

Contents lists available at ScienceDirect

Bone

journal homepage: www.elsevier.com/locate/bone

Full Length Article

Agonist-induced activation of the S1P receptor 2 constitutes a novel osteoanabolic therapy for the treatment of osteoporosis in mice

Sarah Weske[a], Mithila Vaidya[a], Karin von Wnuck Lipinski[a], Petra Keul[a], Kristina Manthe[a], Christoph Burkhart[b], Gebhard Haberhauer[b], Gerd Heusch[a], Bodo Levkau[a,*]

[a] Institute for Pathophysiology, University Hospital Essen, University of Duisburg-Essen, Germany
[b] Institute of Organic Chemistry, University of Duisburg-Essen, Germany

ARTICLE INFO

Keywords:
Bone formation markers
Bone resorption markers
Osteoblasts
Osteoclasts
Osteoporosis
Sphingosine-1-phosphate
Sphingosine-1-phosphate receptor 2

ABSTRACT

Background and purpose: Osteoporosis is a worldwide epidemic but pharmacological agents to stimulate new bone formation are scarce. We have shown that increasing tissue levels of sphingosine-1-phosphate (S1P) by blocking its degradation by the S1P lyase has pronounced osteoanabolic effect in mouse osteoporosis models by stimulating osteoblast differentiation through the S1P receptor 2 (S1P2). However, S1P lyase inhibitors have side effects complicating potential clinical use. Here, we tested whether direct S1P2 engagement by the S1P2 agonist CYM5520 exerted osteoanabolic potential in estrogen deficiency-induced osteopenia in mice. We compared its efficacy to LX2931, a novel S1P lyase inhibitor currently tested in rheumatoid arthritis.

Experimental approach: CYM5520, LX2931 or vehicle were administered to ovariectomized mice for 6 weeks beginning 5 weeks after ovariectomy, Bone mass, cellular composition and mechanical strength were assessed by microCT, histomorphometry and three point bending tests. Plasma markers of bone metabolism were analyzed by ELISA.

Key results: Therapeutic treatment with CYM5520 and LX2931 clearly increased long bone and vertebral bone mass to impressive 3–5 fold over vehicle in osteopenic ovariectomized mice. As expected, lymphopenia was a side effect of LX2931, whereas none occurred with CYM5520. Consistent with an osteoanabolic effect, CYM5520 increased osteoblast number, osteoid surface and alkaline phosphatase area 2–3 fold over vehicle. Plasma concentrations of the osteoanabolic marker procollagen I C-terminal propeptide were also elevated by CYM5520 and LX2931. LX2931 but not yet CYM5520 increased cortical thickness and mechanical strength without affecting mineral density.

Conclusion and implications: Treatment with a pharmacological S1P2 agonist corrected ovariectomy-induced osteopenia in mice by inducing new bone formation thus constituting a novel osteoanabolic approach to osteoporosis.

1. Introduction

Two hundred million people worldwide are currently suffering from osteoporosis. It is the most common bone disease and affects all age groups, genders, and races and becomes most prevalent in post-menopausal women and men over the age of 50 [1,2]. Characterized by low bone mass and deteriorating quality of bone tissue, osteoporosis leads to increased risk of fractures with debilitating consequences, high morbidity and, in men, higher mortality [3]. According to the International Osteoporosis Foundation, 1 in 3 women over the age of 50 years and 1 in 5 men will experience osteoporotic fractures in their lifetime. Longer life span and the increasingly aging population have turned osteoporosis into a global epidemic and major public health burden.

The current pharmacological therapy consists with the exception of human parathyroid hormone only of anti-resorptive agents [2,3] but

Abbreviations: ALP, alkaline phosphatase; BMP, bone mineral density; BV/TV, bone volume per tissue volume; Ct.Th., cortical thickness; DOP, 4-deoxypyridoxine; OB/mmBS, Osteoblast per mm bone surface; OPG, osteoprotegerin; OS/BS, osteoid surface per bone surface; OVX, ovariectomy; PICP, procollagen I C-terminal propeptide; PYD, pyridinoline; S1P, sphingosine-1-phosphate; S1P2, sphingosine-1-phosphate receptor 2; Tb.N., trabecular number; Tb.Sp., trabecular separation; Tb.Th., trabecular thickness; WBC, white blood cells; μCT, X-ray micro-computed tomography

* Corresponding author at: Institute for Pathophysiology, West German Heart and Vascular Center, University Hospital Essen, Hufelandstrasse 55, 45122 Essen, Germany.
E-mail address: bodo.levkau@uni-due.de (B. Levkau).

https://doi.org/10.1016/j.bone.2019.04.015
Received 16 January 2019; Received in revised form 9 April 2019; Accepted 23 April 2019
Available online 24 April 2019

decreased bone formation is at least as important as increased bone resorption in osteoporosis. Thus novel osteoanabolic therapies are dearly sought for [1–3].

We have recently shown that modulation of signaling by the bioactive lipid sphingosine-1-phosphate (S1P) may lay the foundation of novel osteoanabolic agents [4].The role of S1P signaling in bone physiology, homeostasis and disease is an area of intense research as it modulates osteoblast-osteoclast cross-talk, regulates osteoclast precursors and exerts multiple effects on osteoblasts [5–10]. We have shown that pharmacological inhibition or genetic deletion of the S1P lyase, the sole enzyme responsible for irreversible S1P degradation in vivo, increased new bone formation and exercised clear osteoanabolic effects in adult aged bone, corrected osteopenia due to estrogen deficiency after ovariectomy (OVX) and rescued from severe osteoporosis secondary to osteoprotegerin (OPG) deletion in mice [4]. We also identified clear associations of serum S1P and bone health in over 4000 human subjects [4]. The pharmacological S1P lyase inhibitor 4-deoxypyridoxine (DOP) that we employed but also several others of this group such as 2-acetyl-4-((1*R*,2*S*,3*R*)-1,2,3,4-tetrahydroxybutyl)imidazole (THI) and the novel LX2931 ((1*E*)-1-(4-((1*R*,2*S*,3*R*)-1,2,3,4-tetrahydroxybutyl)-1*H*-imidazol-2-yl)ethanone oxime) that is tested as candidate drug for rheumatoid arthritis in a phase 2 clinical trial, block S1P lyase activity by competing with vitamin B6 at the pyridoxal-5′-phosphate binding domain of the enzyme [11,12]. Accordingly, side effects from interference with a number of other vitamin B6-dependent enzymes are expected. In addition, S1P lyase inhibitors raise not only S1P concentrations but also those of other sphingolipids such as sphingosine, ceramide and sphingomyelin [13–15] and inhibit important enzymes in the sphingolipid metabolism such as the serine-palmitoyltransferase, the rate-limiting enzyme in sphingomyelin synthesis [16]. Finally, high levels of S1P accumulating after S1P lyase inhibition act on all five S1P receptors, causing immunosuppression through ligand-induced downregulation of S1P receptor 1 [17] and transient bradycardia [18]. All these effects of S1P lyase inhibitors constitute a caveat for broad clinical applications.

In contrast, selective S1P receptor agonism appears to be a much more promising therapeutic option. We have recently identified S1P receptor 2 (S1P2) as responsible for the osteoanabolic effect of S1P on osteoblast differentiation, proliferation and mineralization [4]. Thus we hypothesized that selective S1P2 agonists devoid of S1P lyase inhibitor side effects would offer a more favourable and potentially clinically applicable osteoanabolic therapy. Besides its role in bone homeostasis, S1P2 is involved in vascular tone regulation, kidney and lung perfusion [19,20], mast cell function [21–23] pathological angiogenesis in the retina [24] and integrity of the cochleo-vestibular system [25,26]. Whereas S1P2-related pathologies have become evident only in S1P2-deficienct mice or after treatment with S1P2 antagonists [27,28], none of the available S1P2 agonists has been tested in a disease-related context in vivo. Thus our study had two major aims: 1) to test whether CYM5520, a highly specific S1P2 agonist [29] that was shown to increase bone mass in normal mice [30], had an osteoanabolic effect in ovariectomized mice in vivo, and 2) to compare its effectiveness to that of LX2931, an S1P lyase inhibitor currently tested in rheumatoid arthritis [30] but of unknown osteoanabolic potential.

2. Materials and methods

2.1. Mouse models

Ovariectomized 12 weeks old C57Bl6J mice were purchased from Charles River Laboratories. Mice were housed in SPF cages without any pathogens and with access to mouse chow and water ad libitum in the Central Animal Facility of the University Hospital Essen, Germany. Treatment was started 5 weeks after OVX. 1*E*)-1-(4-((1*R*,2*S*,3*R*)-1,2,3,4-Tetrahydroxybutyl)-1*H*-imidazol-2-yl)ethanone oxime (LX2931) was synthesized according to the known procedure [31] and administered with the drinking water at 200 mg/kg/day for 6 weeks. CYM5520 (Sigma Aldrich, USA) was administered intraperitoneally at 10 mg/kg/day for 5 consecutive days per week for 6 weeks. All procedures were approved by and in accordance with the institutional guidelines of the Landesamt für Natur, Umwelt und Verbraucherschutz NRW, Germany. Animal studies are reported in compliance with the ARRIVE guidelines [32]. The total number of mice used in the whole study was 21. Every effort was taken to minimize the number of animals used and their suffering.

2.2. Randomization and blinding

Animals were randomized for treatment. Data collection and evaluation of all experiments were performed blindly of the group identity.

2.3. Flow cytometry analysis

White blood cell counts were determined in whole blood with a Scil VetABC hematology analyzer. For CD4 and CD8 analysis, red blood cells were lysed with BD PharmLyse™ buffer (BD Biosciences, USA) followed by two washing steps with stain/wash buffer (1% BSA, 0.1% sodium azide in phosphate buffered saline (PBS)) and incubation with BD Horizon™ V500 Anti-Mouse CD45.2 (BD Biosciences), Anti-Mouse CD4-APC and Anti-Mouse CD8a-PE (both Thermo Fisher Scientific, USA) for 30 min at 4 °C in the dark. Cells were then washed once with stain/wash buffer and analyzed for surface marker expression with a Beckman Coulter Gallios flow cytometer.

2.4. μCT analysis

Quantitative microcomputed tomography of femura and vertebrae were performed using a Skyscan x-ray microtomograph 1072 and CT Analyzer version 1.13.5.1 + (Skyscan, Belgium). Femura and vertebrae (L3) of OVX mice were placed in a tightly fitted plastic tube to prevent movement during the scanning. Whole vertebrae were scanned. For the distal femoral metaphysis region, 800 transverse CT slices covering a region of 6.3 mm were acquired. Image acquisition was performed at 70 kV and 114 μA with an angular increment of 0.45° between projections. Voxel size was 8 μm (isotropic). Image reconstruction was done with NRecon software (V.1.6.9.4; Skyscan, Belgium), and appropriate corrections were applied. Trabecular bone was manually segmented from cortical bone, and trabecular bone parameters were analyzed over 126 slices (1.06 mm), starting 50 slices distal from the growth plate of femura and analyzed over 100 slices (0.84 mm) through the cranial and middle isolateral surface of the vertebrae. For analysis of the femoral midshaft, a region of 0.4 mm in length covering the exact middle of the femura in the mid-diaphysis was analyzed. This region was then used to calculate diaphyseal parameters such as cortical thickness (Ct.Th.) and bone mineral density (BMD). Image acquisition was performed at 70 kV and 114 μA with an angular increment of 0.45° between projections. Voxel size was 19 μm (isotropic). Density calibration was performed against hydroxyapatite phantoms with densities of 250 mg/cm^3 and 750 mg/cm^3. Analyses were performed in agreement with guidelines for assessment of bone microstructure in rodents using micro-CT [33].

2.5. Mechanical testing

The three-point bending test to failure of the femura was performed using a Material Testing System Shimadzu EZ Test EZ-SX device. Load and deflection curves were collected by TrapeziumX Software (both from Shimadzu, Japan). A support span of 5 mm at the bottom of the femura was used, and the load was applied at the midpoint of the posterior aspect of the femura. All tests were performed using a 500 N load cell at a constant loading rate of 3 mm/min. Data were collected every 5 ms. The ultimate force and stiffness were obtained directly from the load and deflection curves. The elastic modulus and ultimate stress

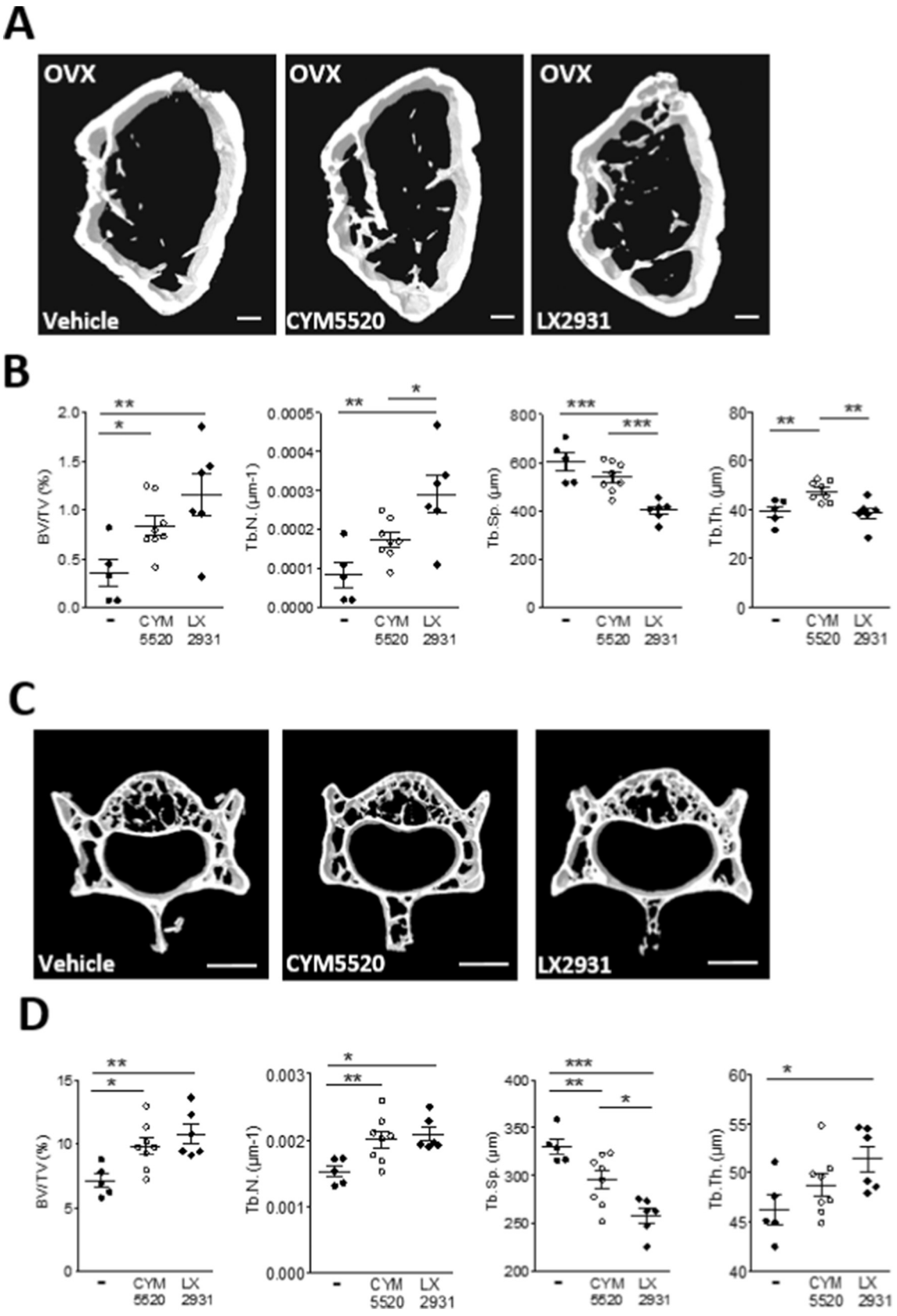

Fig. 1. CYM5520 and LX2931 treatment of OVX mice increase trabecular bone volume.

A Representative µCT images of femoral metaphysis of vehicle-, CYM5520- and LX2931-treated OVX mice. Scale bars: 350 µm. **B** µCT analysis of the spongiosa of the femoral metaphysis of vehicle, CYM5520 and LX2931-treated OVX mice. Quantification of trabecular BV/TV, Tb.N., Tb.Sp. and Tb.Th. are shown.(n = 5,8,6) **C** Representative µCT images of L3 vertebrae of vehicle-, CYM5520- and LX2931-treated OVX mice. Scale bars: 1000 µm. **D** µCT analysis of the spongiosa of the vertebrae of vehicle, CYM5520 and LX2931-treated OVX mice. Quantification of trabecular BV/TV, Tb.N., Tb.Sp. and Tb.Th. are shown.(n = 5,8,6) Data are presented as mean ± s.e.m. One-way ANOVA with Tukey's multiple-comparisons tests were performed. *P < .05; **P < .01; ***P < .001.

were calculated based on the formulae for elastic modulus = KL3/(48 Imin) and ultimate stress = FultLc/(4 lmin). K = stiffness; L = Gauge-length; I = moment of inertia; Fult = ultimate force; Lc = bone radius.

2.6. Histology and histomorphometry

Cryosectioning was performed, as described [34]. In brief, the mouse femur was harvested and the distal part snap-frozen in the embedding medium (C-EM001, Section Lab Co. Ltd., Japan) using liquid nitrogen. Cryosections (5 μm) were cut using a Leica CM 1850 cryotome with disposable stainless steel blades (Feather Microtome Blades, Type N35) and a cryosection preparation kit (C-EM001-C3, Section Lab Co. Ltd., Japan), as described [34]. The bone sections were stored at −80 °C until staining. For staining, cryosections were thawed at room temperature, air dried, washed with 100% ethanol for 5 min to remove the embedding medium and fixed for 5 min in 4.5% formaldehyde (Roti Histofix, Roth, Germany). The sections were then stained for osteoid using a modified McNeal Tetrachrome staining method. Briefly, cryosections were air dried and placed in 5% Tetrachrome solution for 15 min, washed twice in double distilled water and mounted with Faramount aqueous mounting medium. Alkaline phosphatase (ALP) histochemistry was performed according to a modified protocol [35]. Shortly, cryosections were air dried and placed in 1% MgCl 100 mM Tris pH 9.2 at room temperature for 4 h, rinsed in 0.2% Twee-20/PBS for 10 min and then washed in PBS for 10 min. The sections were incubated for 30 min at 37 °C in ALP substrate solution (100 mM Tris buffer, pH 9.2, containing 0.2 mg/ml naphthol AS-MX phosphate dissolved in *N*,*N*-dimethylformamide and 0.4 mg/ml Fast Red TR), washed with distilled water and mounted with Faramount aqueous mounting medium. Bone static histomorphometric analyses for ALP area/bone area were performed using Bioquant Osteo 2009 V9.0 software (Bioquant, USA). At least 2 sections per animal were analyzed by measuring the bone parameters specifically in the subepiphyseal region. Bone histomorphometric parameters were calculated according to the standardized nomenclature for bone histomorphometry [36].

2.7. Enzyme-linked immunosorbent assay (ELISA)

DueSet mouse Osteoprotegerin/TNFRSF11b ELISA (R&D Systhems, USA), pyridinoline (PYD) ELISA (BlueGene Biotech, China) and Procollagen I C-Terminal Propeptide ELISA (Cloud-Clone Corp., USA) were performed according to manufacturer's instructions.

2.8. Statistical analysis

Statistical significances of differences between groups were evaluated by one-way ANOVA with a Tukey's multiple-comparisons test or Two-tailed *t*-test (GraphPad Prism 5.0; GraphPad Software, USA). Data were tested for normality and equal variance before analysis. All results were expressed as means ± standard error of the mean (s.e.m.). $^{*}P < .05$; $^{**}P < .01$; $^{***}P < .001$.

3. Results

3.1. The S1P2 agonist CYM5520 and the S1P lyase inhibitor LX2931 correct osteopenia in OVX mice

Osteopenia after OVX in mice is a recognized model of human estrogen deficiency-induced osteoporosis in post-menopausal women [37]. Using this model, treatment with CYM5520 or LX2931 was started 5 weeks after OVX in an approach to assess therapeutic rather than prophylactic effects as explored earlier for DOP [4]. After 6 weeks of CYM5520 treatment, micro-CT (μCT) analysis of the long bones (femur) was performed and revealed 3.38 fold higher trabecular bone volume/tissue volume (BV/TV), 2.84 fold higher trabecular number (Tb.N.) and 1.25 fold higher trabecular thickness compared to vehicle-treated mice (Fig. 1A, B). Trabecular separation (Tb.Sp.) was not altered (Fig. 1B). Micro-CT analysis of the long bones of mice treated with LX2931 for the same time revealed that BV/TV was 5.0 fold higher and Tb.N. 5.07 fold higher, respectively, compared to the vehicle-treated control. Trabecular thickness (Tb.Th.) was not altered, and Tb.Sp. was 32.7% lower than with vehicle (Fig. 1A, B). Micro-CT analysis of the vertebrae (L3) of the same CYM5520 and LX2931 treated OVX mice demonstrated a similar pattern. CYM5520 treatment resulted in a 1.38 fold higher BV/TV and 1.32 fold higher Tb.N. Trabecular thickness was not altered, and Tb.Sp. was 11% lower than with vehicle (Fig. 1C, D). The analysis of the vertebrae of LX2931 treated OVX mice revealed that BV/TV was 1.58 fold higher, Tb.N. 1.41 fold higher and Tb.Th. 1.11 fold higher, respectively, compared to vehicle-treated mice. Tb.Sp. was 32.8% lower than with vehicle (Fig. 1C, D). LX2931 exhibited a slightly more potent effect than CYM5520 in Tb.N. and Tb.Sp. but was equipotent in the increase of BV/TV.

3.2. CYM5520 and LX2931 stimulate osteoblast activity in vivo

We next examined whether or not higher osteoblast activity caused the increase in trabecular bone volume with CYM5520 and LX2931 treatment. We observed a 2.46 fold higher osteoid surface per bone surface (OS/BS) in CYM5520-treted mice and a 2.22 fold higher one in LX2931-treated mice compared to vehicle-treated controls (Figs. 2A, 4B). Interestingly, the number of OB per mm BS was 1.53 fold higher in CYM5520-treated but was not altered in LX2931-treated OVX mice (Fig. 2C). Moreover, we observed a 2.23 fold higher alkaline phosphatase (ALP) area per bone area in CYM5520-treated OVX mice as a measure of osteoblast presence and activity (Fig. 2D). ALP area was not altered in LX2931 treated mice (Fig. 2E). We also measured plasma concentrations of procollagen I C-terminal propeptide (PICP), a marker for osteoblast activity in vivo. PICP was 1.33 fold higher in CYM5520-treted mice and 1.76 fold higher in LX2931-treated mice than in the vehicle group (Fig. 2F). PICP levels with LX2931 were higher than those with CYM5520 (Fig. 2F).

3.3. Effects of CYM5520 and LX2931 on cortical thickness and mechanical bone parameters

We then tested whether or not CYM5520 and LX2931 treatment caused an increase in cortical thickness, bone mineral density and mechanical bone strength. Indeed, Ct.Th. was 1.08 fold higher in LX2931-treated OVX mice than in the vehicle group (Fig. 3A). CYM5520 treatment had no effect (Fig. 3A). BMD was not altered in CYM5520- or LX2931-treated mice compared to vehicle (Fig. 3B). We next assessed mechanical bone strength in a three-point bending test of the femur (Fig. 3C). In LX2931-treated OVX mice, the ultimate force was 1.26 fold higher and the stiffness 1.28 fold higher than in the vehicle group (Fig. 3D). The elastic modulus and ultimate stress were unaffected (Fig. 3D). CYM5520 had no effect (Fig. 3D).

3.4. LX2931 but not CYM5520 causes immunosuppression

Immunosuppression is a common feature of high S1P levels caused by S1P lyase inhibition or genetic deletion, and peripheral blood lymphopenia is a reliable readout for the magnitude of the effect. No data are available on the effects of S1P2 agonism on peripheral blood lymphocytes. We thus analyzed peripheral white blood cells (WBC) and CD4+ and CD8+ T-cells in LX2931- and CYM5520-treated mice. WBC were ~50% lower in LX2931-treted mice compared to vehicle-treated mice but were unaltered in CYM5520-treated mice excluding lymphopenia as a side effect (Fig. 4A). Flow cytometry demonstrated that both CD4+ and CD8+ lymphocytes were ~90% lower in LX2931-treated OVX mice than in vehicle controls (Fig. 4B, C). Again, CYM5520 did not alter CD4+ and CD8+ cell counts (Fig. 4B, C).

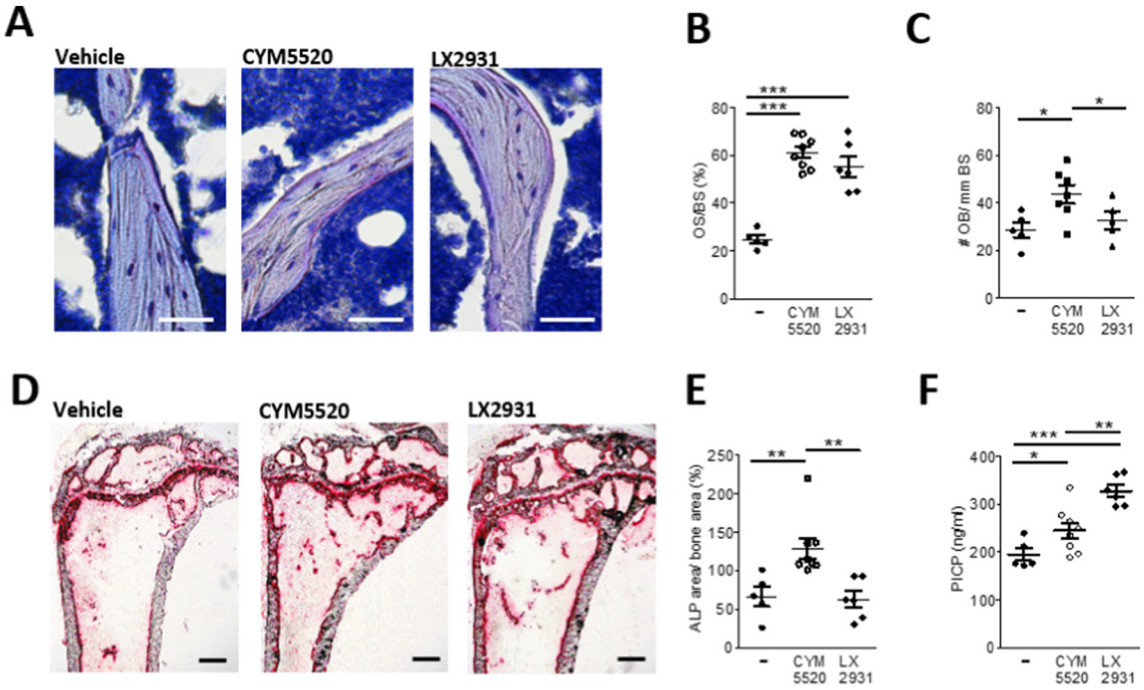

Fig. 2. CYM5520 and LX2931 increase osteoblast activity in OVX mice.
A Representative pictures of tetrachrome staining of trabecular bone of femura of vehicle-, CYM5520- and LX2931-treated OVX mice. Scale bars: 400 µm. **B** Histomorphometric analysis of OS/BS of vehicle, CYM5520 and LX2931-treated OVX mice. (n = 5,8,6) **C** Histomorphometric analysis of number of OB/mm BS of vehicle-, CYM5520- and LX2931-treated OVX mice. (n = 5,7,5) **D** Representative pictures of ALP staining of femura of vehicle-, CYM5520- and LX2931-treated OVX mice. Scale bars: 200 µm. **E** Histomorphometric analysis of ALP area/bone area of vehicle-, CYM5520- and LX2931-treated OVX mice. (n = 5,8,6) **F** PICP plasma concentration in vehicle-, CYM5520- and LX2931-treated OVX mice. (n = 5,8,6) Data are presented as mean ± s.e.m. One-way ANOVA with Tukey's multiple-comparisons tests (A-E) were performed. $*P < .05$; $**P < .01$; $***P < .001$.

4. Discussion

In our study, we have demonstrated for the first time successful osteoanabolic therapy with the S1P2 agonist CYM5520 in OVX-induced osteopenia in mice. CYM5520 has been previously shown to increase BV/TV in young (8 weeks-old) healthy mice [30]. In our study, the effect of CYM5520 was comparable to that of the S1P lyase inhibitor LX2931 (currently in a phase 2 clinical trial for rheumatoid arthritis). CYM5520 and LX2931 were not always equipotent. Both were similarly effective in major readouts such as BV/TV but LX2931 was more effective in increasing cortical thickness and ultimate force. However, there were also parameters such as OB numbers and ALP where CYM5520 was superior to LX2931. The most relevant explanation for these differences is that LX2931 increases the amounts of the genuine S1P that acts on all S1P receptors, several of which are involved in bone physiology with sometimes overlapping effects on osteoblast behavior [31]. In contrast, CYM5520 is highly specific for S1P2 [29]. LX2931 inhibits the S1P lyase through the same mechanism as DOP, the inhibitor we have used previously for the same purpose in bone studies [4]. Thus, unsurprisingly, the osteoanabolic effect of LX2931 was comparable to that of DOP in the OVX model. Besides testing LX2931 as another substance of the same class as DOP, we employed it mainly as a control and benchmark for CYM5520 as our main goal was to establish a S1P2-based osteoanabolic treatment without immunosuppressive effects. Indeed, S1P2 activation does not have immunosuppressive effects because lymphocyte trafficking is exclusively mediated by the S1P1 receptor [38]. Furthermore, CYM5520 is highly specific for S1P2 (EC50 0.48 µM for S1P2 and > 10 µM for S1P1) [29] and exerted no effect on peripheral lymphocyte numbers.

Our most exciting finding was that treatment with CYM5520 was similarly efficient as S1P lyase inhibition in the treatment of OVX-induced osteopenia based on the increase in bone mass. Although we did not perform dynamic histomorphometry to assess new bone formation as in our previous work with DOP [4]. Despite this limitation, we observed an increase in actual OB numbers and osteoid surface per bone surface, and we found higher procollagen plasma concentrations in plasma as readout for elevated OB activity in vivo.

We have selected S1P2 as pharmacological target in osteoporosis based on our previous work that identified several osteoblast functions such as differentiation, proliferation and mineralization to be stimulated by the S1P in wild type but not S1P2-deficient osteoblasts and the appearance of osteopenia in S1P2-deficient mice. The CYM5520 dose was chosen based on that of other S1P receptor agonists and antagonists such as W146 that exerted an effect in vivo [39]. It was 10-fold higher than previously used in healthy young mice [30], and caused a higher (3.38-fold) increase in BV/TV compare to the 1.6-fold observed before [30]. This and the absence of lymphopenia leave ample room for further pharmacological optimization.

In our previous work we have shown that S1P2 also induced OPG production in vitro and in vivo suggesting an additional anti-resorptive effect [4]. Here, we have also observed increased plasma OPG concentrations with CYM5520 and LX2931 (Suppl. Fig. 1A). However, the plasma marker of osteoclast activity PYD and TRAP positivity in situ remained unchanged (Suppl. Fig. 1B, C) suggesting a less prominent contribution.

In summary, our study has identified a highly promising osteoanabolic potential of pharmacological S1P2 agonists in the therapy of OVX-induced osteopenia without immunosuppression as a side effect. This may pave the road for further preclinical and clinical testing and offer an entirely novel pharmacological approach to osteoporosis therapy.

Supplementary data to this article can be found online at https://doi.org/10.1016/j.bone.2019.04.015.

Acknowledgments

This work was supported in part by grant number 195 from the

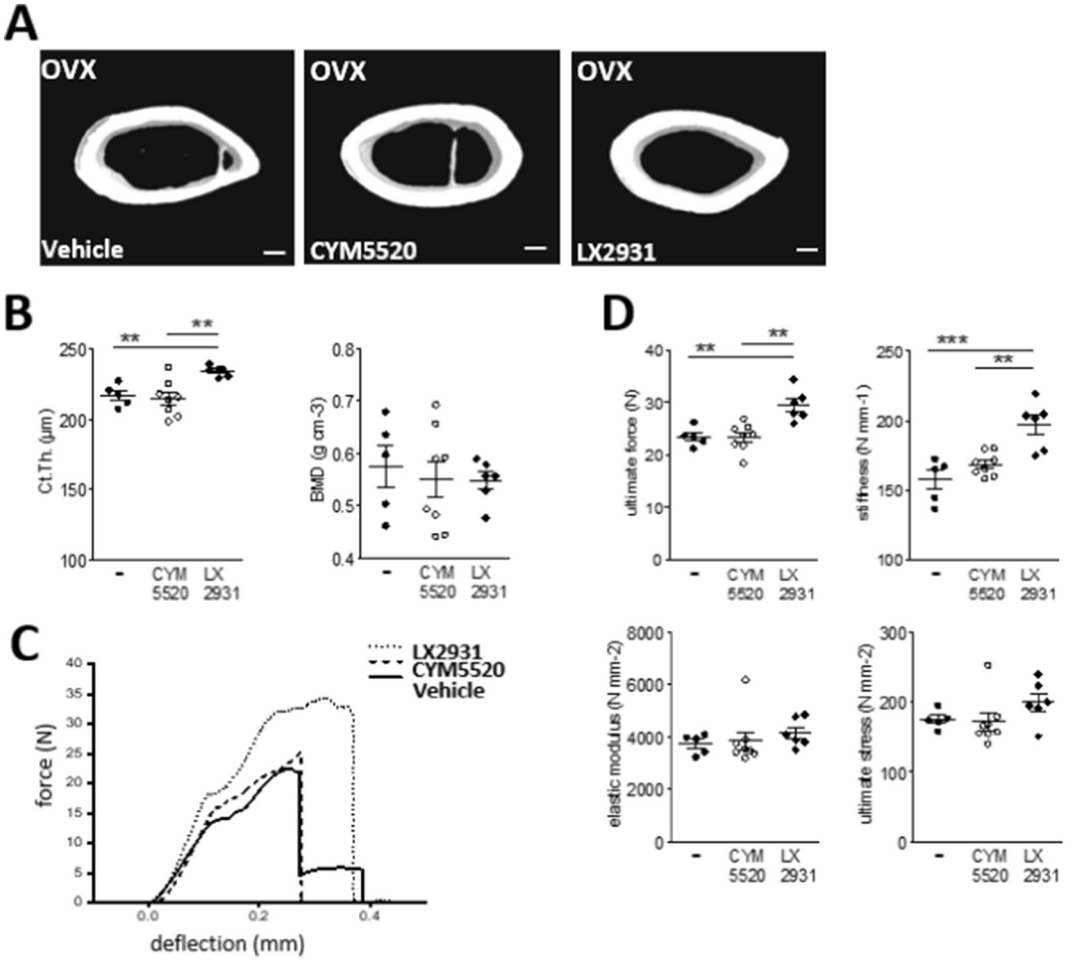

Fig. 3. Effects of CYM5520 and LX2931 on cortical thickness and mechanical bone parameters.
A Representative µCT images of the femoral midshaft of vehicle-, CYM5520- and LX2931-treated OVX mice. Scale bars: 200 µm. **B** Quantification of Ct.Th. and BMD of vehicle-, CYM5520- and LX2931-treated OVX mice. (n = 5,8,6) **C** Representative curves of the three-point bending test of femura of vehicle-, CYM5520- and LX2931-treated OVX mice. **D** Ultimate force, stiffness, elastic modulus and ultimate stress in the three-point bending test of the femoral midshafts of vehicle-, CYM5520- and LX2931-treated OVX mice. (n = 5,8,6) Data are presented as mean ± s.e.m. One-way ANOVA with Tukey's multiple-comparisons tests were performed. $*P < .05$; $**P < .01$; $***P < .001$.

Elsbeth Bonhoff Stiftung, Berlin, Germany (B.L.). We thank Petra Schneider and Helma Kallweit for excellent technical help.

Author contributions

S.W., M.V., K.vW-L., P.K., K.M. and C.B. performed research and collected data. G.Ha. and G.He. contributed vital reagents or analytical tools and interpreted data. S.W., M.V. and B.L. designed research, analyzed and interpreted data and wrote the manuscript.

Disclosure

The authors have no financial conflicts of interest.

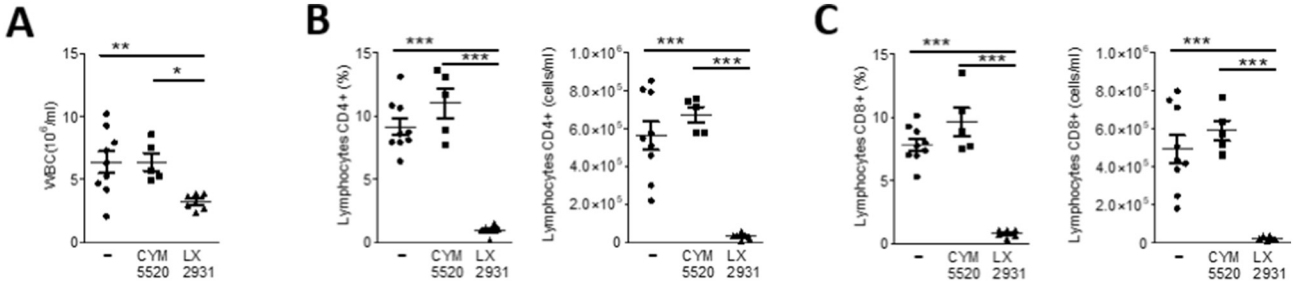

Fig. 4. Flow cytometry analysis of the peripheral blood of CYM5520- and LX2931-treated OVX mice.
A WBC counts of vehicle-, CYM5520- and LX2931-treated OVX mice. (n = 9,5,7) **B** Percentage distribution (left) and total cell numbers (right) of CD45 + /CD4 + cells in peripheral blood of vehicle-, CYM5520- and LX2931-treated OVX mice. (n = 9,5,6) **C** Percentage distribution (left) and total cell numbers (right) of CD45 + / CD8 + cells in peripheral blood of vehicle-, CYM5520- and LX2931-treated OVX mice. (n = 9,5,6) Data are presented as mean ± s.e.m. One-way ANOVA with Tukey's multiple-comparisons tests were performed. $*P < .05$; $**P < .01$; $***P < .001$.

References

[1] F. Cosman, S.J. de Beur, M.S. LeBoff, E.M. Lewiecki, B. Tanner, S. Randall, et al., Clinician's guide to prevention and treatment of osteoporosis, Osteoporos. Int. 25 (10) (2014) 2359–2381.

[2] T. Sozen, L. Ozisik, N.C. Basaran, An overview and management of osteoporosis, Eur. J. Rheumatol. Inflamm. 4 (1) (2017) 46–56.

[3] N.C. Wright, A.C. Looker, K.G. Saag, J.R. Curtis, E.S. Delzell, S. Randall, et al., The recent prevalence of osteoporosis and low bone mass in the United States based on bone mineral density at the femoral neck or lumbar spine, J. Bone Miner. Res. 29 (11) (2014) 2520–2526.

[4] S. Weske, M. Vaidya, A. Reese, K. von Wnuck Lipinski, P. Keul, J.K. Bayer, et al., Targeting sphingosine-1-phosphate lyase as an anabolic therapy for bone loss, Nat. Med. 24 (5) (2018) 667–678.

[5] A. Grey, Q. Chen, K. Callon, X. Xu, I.R. Reid, J. Cornish, The phospholipids sphingosine-1-phosphate and lysophosphatidic acid prevent apoptosis in osteoblastic cells via a signaling pathway involving G(i) proteins and phosphatidylinositol-3 kinase, Endocrinology 143 (12) (2002) 4755–4763.

[6] M. Ishii, J. Kikuta, Y. Shimazu, M. Meier-Schellersheim, R.N. Germain, Chemorepulsion by blood S1P regulates osteoclast precursor mobilization and bone remodeling in vivo, J. Exp. Med. 207 (13) (2010) 2793–2798.

[7] J. Keller, P. Catala-Lehnen, A.K. Huebner, A. Jeschke, T. Heckt, A. Lueth, et al., Calcitonin controls bone formation by inhibiting the release of sphingosine 1-phosphate from osteoclasts, Nat. Commun. 5 (2014) 5215.

[8] E. Matsuzaki, S. Hiratsuka, T. Hamachi, F. Takahashi-Yanaga, Y. Hashimoto, K. Higashi, et al., Sphingosine-1-phosphate promotes the nuclear translocation of beta-catenin and thereby induces osteoprotegerin gene expression in osteoblast-like cell lines, Bone 55 (2) (2013) 315–324.

[9] J. Ryu, H.J. Kim, E.J. Chang, H. Huang, Y. Banno, H.H. Kim, Sphingosine 1-phosphate as a regulator of osteoclast differentiation and osteoclast-osteoblast coupling, EMBO J. 25 (24) (2006) 5840–5851.

[10] C. Sato, T. Iwasaki, S. Kitano, S. Tsunemi, H. Sano, Sphingosine 1-phosphate receptor activation enhances BMP-2-induced osteoblast differentiation, Biochem. Biophys. Res. Commun. 423 (1) (2012) 200–205.

[11] H. Le Stunff, S. Milstien, S. Spiegel, Generation and metabolism of bioactive sphingosine-1-phosphate, J. Cell. Biochem. 92 (5) (2004) 882–899.

[12] P.P. Van Veldhoven, Sphingosine-1-phosphate lyase, Methods Enzymol. 311 (2000) 244–254.

[13] P. Bandhuvula, H. Fyrst, J.D. Saba, A rapid fluorescence assay for sphingosine-1-phosphate lyase enzyme activity, J. Lipid Res. 48 (12) (2007) 2769–2778.

[14] M. Ohtoyo, M. Tamura, N. Machinaga, F. Muro, R. Hashimoto, Sphingosine 1-phosphate lyase inhibition by 2-acetyl-4-(tetrahydroxybutyl)imidazole (THI) under conditions of vitamin B6 deficiency, Mol. Cell. Biochem. 400 (1–2) (2015) 125–133.

[15] S.W. Paugh, B.S. Paugh, M. Rahmani, D. Kapitonov, J.A. Almenara, T. Kordula, et al., A selective sphingosine kinase 1 inhibitor integrates multiple molecular therapeutic targets in human leukemia, Blood 112 (4) (2008) 1382–1391.

[16] N. Hagen-Euteneuer, D. Lutjohann, H. Park, A.H. Merrill Jr., G. van Echten-Deckert, Sphingosine 1-phosphate (S1P) lyase deficiency increases sphingolipid formation via recycling at the expense of de novo biosynthesis in neurons, J. Biol. Chem. 287 (12) (2012) 9128–9136.

[17] S.R. Schwab, J.P. Pereira, M. Matloubian, Y. Xu, Y. Huang, J.G. Cyster, Lymphocyte sequestration through S1P lyase inhibition and disruption of S1P gradients, Science 309 (5741) (2005) 1735–1739.

[18] M.G. Sanna, J. Liao, E. Jo, C. Alfonso, M.Y. Ahn, M.S. Peterson, et al., Sphingosine 1-phosphate (S1P) receptor subtypes S1P1 and S1P3, respectively, regulate lymphocyte recirculation and heart rate, J. Biol. Chem. 279 (14) (2004) 13839–13848.

[19] J.N. Lorenz, L.J. Arend, R. Robitz, R.J. Paul, A.J. MacLennan, Vascular dysfunction in S1P2 sphingosine 1-phosphate receptor knockout mice, Am. J. Phys. Regul. Integr. Comp. Phys. 292 (1) (2007) R440–R446.

[20] A. Skoura, T. Hla, Regulation of vascular physiology and pathology by the S1P2 receptor subtype, Cardiovasc. Res. 82 (2) (2009) 221–228.

[21] P.S. Jolly, M. Bektas, A. Olivera, C. Gonzalez-Espinosa, R.L. Proia, J. Rivera, et al., Transactivation of sphingosine-1-phosphate receptors by FcepsilonRI triggering is required for normal mast cell degranulation and chemotaxis, J. Exp. Med. 199 (7) (2004) 959–970.

[22] C.A. Oskeritzian, N.C. Hait, P. Wedman, A. Chumanevich, E.M. Kolawole, M.M. Price, et al., The sphingosine-1-phosphate/sphingosine-1-phosphate receptor 2 axis regulates early airway T-cell infiltration in murine mast cell-dependent acute allergic responses, J. Allergy Clin. Immunol. 135 (4) (2015) 1008–18 e1.

[23] C.A. Oskeritzian, M.M. Price, N.C. Hait, D. Kapitonov, Y.T. Falanga, J.K. Morales, et al., Essential roles of sphingosine-1-phosphate receptor 2 in human mast cell activation, anaphylaxis, and pulmonary edema, J. Exp. Med. 207 (3) (2010) 465–474.

[24] A. Skoura, T. Sanchez, K. Claffey, S.M. Mandala, R.L. Proia, T. Hla, Essential role of sphingosine 1-phosphate receptor 2 in pathological angiogenesis of the mouse retina, J. Clin. Invest. 117 (9) (2007) 2506–2516.

[25] D.R. Herr, M.J. Reolo, Y.X. Peh, W. Wang, C.W. Lee, R. Rivera, et al., Sphingosine 1-phosphate receptor 2 (S1P2) attenuates reactive oxygen species formation and inhibits cell death: implications for otoprotective therapy, Sci. Rep. 6 (2016) 24541.

[26] M. Kono, I.A. Belyantseva, A. Skoura, G.I. Frolenkov, M.F. Starost, J.L. Dreier, et al., Deafness and stria vascularis defects in S1P2 receptor-null mice, J. Biol. Chem. 282 (14) (2007) 10690–10696.

[27] V.A. Blaho, T. Hla, An update on the biology of sphingosine 1-phosphate receptors, J. Lipid Res. 55 (8) (2014) 1596–1608.

[28] K.V. Blankenbach, S. Schwalm, J. Pfeilschifter, D. Meyer Zu Heringdorf, Sphingosine-1-phosphate receptor-2 antagonists: therapeutic potential and potential risks, Front. Pharmacol. 7 (2016) 167.

[29] H. Satsu, M.T. Schaeffer, M. Guerrero, A. Saldana, C. Eberhart, P. Hodder, et al., A sphingosine 1-phosphate receptor 2 selective allosteric agonist, Bioorg. Med. Chem. 21 (17) (2013) 5373–5382.

[30] K. Higashi, E. Matsuzaki, Y. Hashimoto, F. Takahashi-Yanaga, A. Takano, H. Anan, et al., Sphingosine-1-phosphate/S1PR2-mediated signaling triggers Smad1/5/8 phosphorylation and thereby induces Runx2 expression in osteoblasts, Bone 93 (2016) 1–11.

[31] J.T. Bagdanoff, M.S. Donoviel, A. Nouraldeen, M. Carlsen, T.C. Jessop, J. Tarver, et al., Inhibition of sphingosine 1-phosphate lyase for the treatment of rheumatoid arthritis: discovery of (E)-1-(4-((1R,2S,3R)-1,2,3,4-tetrahydroxybutyl)-1H-imidazol-2-yl)ethanone oxime (LX2931) and (1R,2S,3R)-1-(2-(isoxazol-3-yl)-1H-imidazol-4-yl)butane-1,2,3,4-tetraol (LX2932), J. Med. Chem. 53 (24) (2010) 8650–8662.

[32] C. Kilkenny, W.J. Browne, I.C. Cuthill, M. Emerson, D.G. Altman, Improving bioscience research reporting: the ARRIVE guidelines for reporting animal research, J. Pharmacol. Pharmacother. 1 (2) (2010) 94–99.

[33] M.L. Bouxsein, S.K. Boyd, B.A. Christiansen, R.E. Guldberg, K.J. Jepsen, R. Muller, Guidelines for assessment of bone microstructure in rodents using micro-computed tomography, J. Bone Miner. Res. 25 (7) (2010) 1468–1486.

[34] T. Kawamoto, K. Kawamoto, Preparation of thin frozen sections from nonfixed and undecalcified hard tissues using Kawamot's film method (2012), Methods Mol. Biol. 1130 (2014) 149–164.

[35] D. Miao, A. Scutt, Histochemical localization of alkaline phosphatase activity in decalcified bone and cartilage, J. Histochem. Cytochem. 50 (3) (2002) 333–340.

[36] D.W. Dempster, J.E. Compston, M.K. Drezner, F.H. Glorieux, J.A. Kanis, H. Malluche, et al., Standardized nomenclature, symbols, and units for bone histomorphometry: a 2012 update of the report of the ASBMR Histomorphometry Nomenclature Committee, J. Bone Miner. Res. 28 (1) (2013) 2–17.

[37] R.T. Turner, A. Maran, S. Lotinun, T. Hefferen, G.L. Evans, M. Zhang, et al., Animal models for osteoporosis, Rev. Endocr. Metab. Disord. 2 (2001) 117–127.

[38] M. Matloubian, C.G. Lo, G. Cinamon, M.J. Lesneski, Y. Xu, V. Brinkmann, et al., Lymphocyte egress from thymus and peripheral lymphoid organs is dependent on S1P receptor 1, Nature 427 (6972) (2004) 355–360.

[39] M.G. Sanna, S.K. Wang, P.J. Gonzalez-Cabrera, A. Don, D. Marsolais, M.P. Matheu, et al., Enhancement of capillary leakage and restoration of lymphocyte egress by a chiral S1P1 antagonist in vivo, Nat. Chem. Biol. 2 (8) (2006) 434–441.